Structure and metastability of mesoscopic vacancy and interstitial loop defects in iron and tungsten

2008 J. Phys.: Condens. Matter 20 345214

(http://iopscience.iop.org/0953-8984/20/34/345214)

J. Phys.: Condens. Matter **20** (2008) 345214 (10pp) doi:10.1088/0953-8984/20/34/345214

Structure and metastability of mesoscopic vacancy and interstitial loop defects in iron and tungsten

M R Gilbert[1,2], S L Dudarev[1,3], P M Derlet[4] and D G Pettifor[2]

[1] EURATOM/UKAEA Fusion Association, Culham Science Centre, Oxfordshire OX14 3DB, UK
[2] Department of Materials, University of Oxford, Parks Road, Oxford OX1 3PH, UK
[3] Department of Physics, Imperial College, Exhibition Road, London SW7 2AZ, UK
[4] Paul Scherrer Institute, CH-5232 Villigen PSI, Switzerland

E-mail: mark.gilbert@ukaea.org.uk

Received 11 February 2008, in final form 12 June 2008
Published 1 August 2008
Online at stacks.iop.org/JPhysCM/20/345214

Abstract

The most recent observations of dynamical time-dependent fluctuating behaviour of mesoscopic radiation defects in body-centred cubic metals (Arakawa *et al* 2006 *Phys. Rev. Lett.* **96** 125506; 2007 *Science* **318** 956–9; Yao *et al* 2008 *Phil. Mag.* at press) have highlighted the need to develop adequate quantitative models for the structural stability of defects in the *mesoscopic* limit where defects are accessible to direct *in situ* electron microscope imaging. In pursuit of this objective, we investigate and compare several types of mesoscopic vacancy and interstitial defects in iron and tungsten by simulating them using recently developed many-body interatomic potentials. We show that the mesoscopic vacancy dislocation loops observed in ion-irradiated materials are, without exception, metastable with respect to the transformation into spherical voids, but that the rate of this transformation and even the specific type of the transformation mechanism depend on the defect size and the properties of the material.

(Some figures in this article are in colour only in the electronic version)

1. Introduction

Ferritic-martensitic bcc (body-centred cubic) iron-based steels and tungsten are the main candidate materials for structural and plasma facing components of future deuterium–tritium fusion power plants. During the lifetime of components these metals will be subject to a significant flux of neutrons, resulting in radiation damage due to knock-on cascades. Collision cascades lead to the production of interstitial and vacancy defects, which form defect clusters, either in the core of the cascade itself, or as a result of subsequent migration and interactions [4, 5].

An understanding of the evolution of this damage, which can lead to loss of material integrity, first requires knowledge of the structure and relative stability of the different types of interstitial and vacancy defects formed. In particular, the present work investigates the electron microscopy observation of unexpected stability of planar vacancy loops in ion-irradiated bcc metals, as well as the corresponding low-yield of visible (in electron microscope images) loop defects in collision cascade events compared to other metals such as face-centred cubic (fcc) copper.

There is a significant amount of experimental work on the damage produced by heavy-ion bombardment of iron published in the literature, for which extensive reviews can be found in [6–8]. For tungsten experimental information is less extensive but Häussermann [9], and Jäger and Wilkens [10] have investigated defects formed by irradiating this metal. Further work on defects formed by heavy-ion bombardment of iron [11–13] was recently extended to *in situ* electron microscope observations of time-dependent fluctuating dynamics of radiation defects in thin foils [1–3]. In [3], Yao *et al* have observed the formation of vacancy loops in heavy-ion irradiated foils of Fe and FeCr-alloy. In the current paper we specifically concentrate on the investigation of vacancy and interstitial defects in the mesoscopic limit

(where a defect may contain up to several hundred individual self-interstitial atoms or vacancies) since these defects are observed in electron microscope examinations of irradiated foils [8].

Alongside the experimental work there have been several computational investigations of irradiation damage. In 1985, molecular dynamics (MD) simulations of model fcc and bcc metals by Matthai and Bacon [14] were the first to demonstrate that vacancy defects could form in the thermal spikes associated with irradiation cascades, providing the concentration of vacancies was sufficiently high. More than a decade later, Soneda and Diaz de la Rubia [15] made a significant step in the understanding of evolution of cascades in Fe through the combined use of MD and kinetic Monte Carlo (kMC) simulations. They observed that single vacancies migrated significantly more slowly than self-interstitial atom defects. kMC simulations also showed that vacancies only started clustering once the self-interstitial atom defects became rare, either as a result of the latter migrating away from the centre of the cascade, or due to recombination. Additionally, Soneda and Diaz de la Rubia [15] concluded that the $\mathbf{b} = a/2\langle 111\rangle$ planar self-interstitial loops were the most stable interstitial cluster configuration in Fe. They noted that spherical voids had the highest binding energy, and therefore the lowest formation energy, of all the vacancy cluster configurations. Similar findings were reported in [16].

At the same time, in the simulations of voids and vacancy clusters [15] no collapse of a group of individual vacancies into a vacancy dislocation loop was ever observed, and in the kMC simulations no evidence was found for the formation of large vacancy clusters. An observation of an individual $\langle 100\rangle$ vacancy loop forming directly in a cascade was reported later [17]. More recently Calder *et al* [18] have simulated the formation of $\langle 100\rangle$ vacancy loops in α-iron and showed that the yield of defects increases with both the mass and energy of the primary knock-on atom (PKA) due to the heightened energy density in the cascade region.

Puigvi *et al* [19] performed atomistic simulations of mesoscopic defects in bcc Fe. They analysed the $\mathbf{b} = a/2\langle 111\rangle$ interstitial loops and the so-called closed vacancy loops. This work followed earlier research by Osetsky *et al* on the structure and stability of vacancy and interstitial clusters in bcc Fe and fcc Cu [20].

It is obvious from the literature that little is known about the behaviour of defects in tungsten, either experimentally or from simulations. The present studies address this by direct comparison with a similar metal (Fe) about which much more is known.

To describe interactions between atoms in simulations we primarily used two recently developed many-body interatomic potentials. For iron, we use the Dudarev–Derlet (D–D) 'magnetic' many-body potential developed in [21, 22]. This is a relatively short-range many-body potential derived by taking magnetic interactions between atoms in iron into account. The embedding and the pairwise parts of this potential are made up of a summation of cubic knot functions, which have been fitted to various material properties including the bulk cohesive energy, lattice constant, elastic stiffness constant of different phases, the un-relaxed vacancy formation energy, and the relaxed formation energies of the three high-symmetry self-interstitial atom configurations (see [21] for more detail). As both a check and comparison we have also performed simulations using the popular non-magnetic Fe potential of Mendelev *et al* [23]. Very recently Derlet *et al* [24] have used similar fitting methods to derive interatomic potential parameters for five of the non-magnetic bcc transition metals (V, Nb, Ta, Mo, and W). The parameters for the interatomic interaction between atoms in tungsten described in [24] were used in the present simulations.

The paper is organized as follows. We start by briefly addressing the structure of the defects and the simulation method. Then we compare energies of alternative configurations containing the same number of individual defects (either vacancies or self-interstitial atoms) using molecular statics (MS), and assess the relative stability of the 'competing' defect configurations in iron and tungsten. Subsequently, we estimate the timescales for the formation of defect clusters in cascades, and highlight the extreme difference between the timescales characterizing microstructural evolution of iron and tungsten under irradiation.

2. Vacancy and self-interstitial defects at 0 K

The formation energy $E_{\mathrm{D}}^{\mathrm{f}}$ of a defect configuration is defined as the difference between the minimum energy evaluated for a simulation cell containing the defect, and the energy of a perfect lattice containing the same number of atoms, namely

$$E_{\mathrm{D}}^{\mathrm{f}} = E_{\mathrm{L+D}}^{r}(n) - E_{\mathrm{p}}^{r}(n), \tag{1}$$

where $E_{\mathrm{L+D}}^{r}(n)$ is the energy of a set of n atoms containing the defect and $E_{\mathrm{p}}^{r}(n)$ is the energy of a perfect lattice of n atoms. For the case of a Bravais lattice $E_{\mathrm{p}}^{r}(n)$ is equal to nE_{atom}^{r}, which is n times the energy of a single atom in a lattice (the cohesive energy). In the simulations carried out here the cohesive energy of iron for the Dudarev–Derlet magnetic potential is -4.316 eV per atom (-4.122 eV for Mendelev), whilst in tungsten the cohesive energy per atom is -8.90 eV. From this point onwards we imply the defect formation energy whenever we refer to the energy of a defect. We now evaluate the formation energies of the mesoscopic circular $\mathbf{b} = (a/2)\langle 111\rangle$ and $\mathbf{b} = a\langle 100\rangle$ vacancy and interstitial loops that are frequently observed in ion-irradiated materials. As was noted in 1967 by Johnson for nickel [25], there is an issue as to the stability of vacancy dislocation loops relative to other types of vacancy cluster. To investigate this for Fe and W we also compare the closed (collapsed) vacancy dislocation loop energies with the energies of spherical voids and open loops (planar voids) containing the same number of single vacancy defects.

The formation energies were calculated using molecular static (MS) simulations on lattices with periodic boundary conditions (PBCs). MS is the energy minimization form of molecular dynamics and involves forcing the kinetic energy of the system to decrease, thereby causing the atoms to 'relax'

to a 'frozen' zero-temperature configuration. Each simulation was performed under constant pressure conditions with an orthorhombic geometry that allowed the lattice to expand and contract in each of the three coordinate directions. In the case of the ⟨111⟩ defects this meant the $[1\bar{1}0]$, $[11\bar{2}]$, and [111] coordinate axis directions, while for ⟨100⟩ loop the box was allowed to expand in the normal Cartesian directions. The result of this process was a simulation cell that could change its volume, perhaps in order to accommodate extra atoms, but always remained cuboid.

2.1. Vacancy defects: BCC iron

Constructing the initial configurations of vacancy loops for atomistic simulations is known to present a non-trivial problem, and the only practical solution found so far involved switching between a long-range and a short-range interatomic potential [19]. In this work, to construct open vacancy loops, circular discs of atoms of a given radius were removed from three consecutive (111) ABC planes for $\frac{1}{2}\langle 111\rangle$ loops and two consecutive (100) AB planes for ⟨100⟩ loops. On the other hand, to construct a *closed* vacancy loop, planes of atoms *outside* the loop radius (i.e. in the bulk) were now appropriately *added* to the initial bcc lattice at the mid-way points between the (111) or (100) planes. When these configurations were relaxed, the extra planes in the bulk expanded to a perfect lattice configuration, and a prismatic closed vacancy dislocation loop was created. This procedure did not require the sub-relaxations and sequential applications of long- and short-range interatomic potentials as described in [19], but did produce the desired closed vacancy dislocation loop.

A spherical void was created by removing a sphere of atoms of a given radius. Here we do not consider the possibility of faceting. The simulation cell used for calculations with the Dudarev–Derlet potential consisted of 48 000 atoms, which was large enough to preclude any significant elastic image force effects for the largest defect structures considered. In validation simulations we investigated the formation energy of defects in a range of simulation cell sizes containing up to 0.4 million atoms, and found that there was less than a 1% difference in the energy for simulation cells sizes from around 30 000 atoms up to the maximum size considered. We also note that this implies that surface effects are not very important in the results discussed here. The PBCs used in the simulations mimic the effect of nearby surfaces, i.e. the defect 'sees' itself through the PBCs in the same way that it would experience an image force if it were near a surface, for example in a thin foil. A lattice containing around 30 000 atoms is roughly 7 nm^3 in size, which means that a loop defect was around 14 nm away from itself in the [111] direction (the only defects for which images are significant are the closed vacancy and interstitial loops with their relatively long-range elastic fields, but these only extend in the [111] direction). This shows that our simulations apply to cases in which surfaces do not play a significant role.

For the D–D potential, figure 1 shows the defect energy as a function of defect size, measured in terms of the number

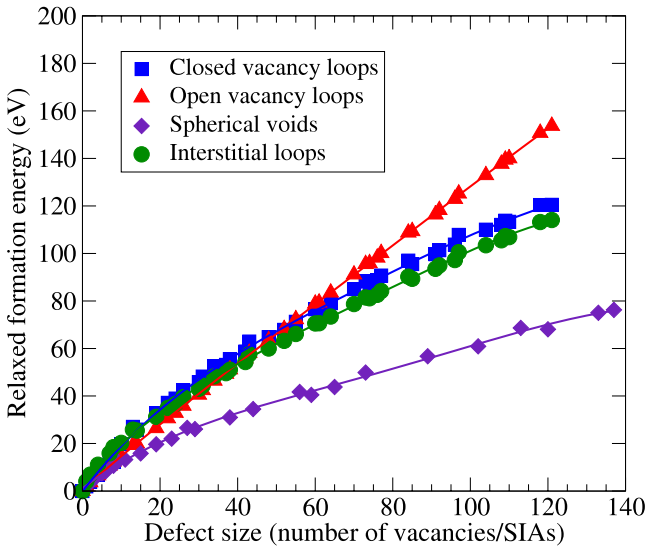

Figure 1. Variation in formation energy of spherical voids and various $\frac{1}{2}\langle 111\rangle$ loop defects in Fe under the Dudarev–Derlet magnetic potential as a function of defect size. The lines represent continuous interpolations between the discrete data points found using atomistic simulations.

of vacancies/interstitials, for all open and closed $\frac{1}{2}\langle 111\rangle$ vacancy loops, spherical voids and $\frac{1}{2}\langle 111\rangle$ interstitial loops. Here the lines represent continuous interpolations between the discrete data points found using atomistic simulations. The graph shows that spherical voids represent the lowest energy configuration for a cluster of vacancies of any size. This agrees with the findings of Soneda and Diaz de la Rubia [15], and Beeler [16]. We see that there is an intersection between the formation energy curves for the open and closed vacancy loops. The cross-over from positive to negative difference between the energies of an open and a closed loop occurs near the 17.7 Å loop diameter, or a 52-vacancy defect, where the closed loop structure becomes energetically more favourable. Below this size an open vacancy loop configuration has lower formation energy. To give a clear illustration of this point, in figure 2 we plot the difference between the formation energies for an open and a closed loop as a function of the loop diameter. For diameters below 5 Å it is effectively impossible to form a closed vacancy loop, as an attempt to form it in a simulation immediately results in the loop opening-up even at 0 K. For loop diameters between 5 Å and 17.7 Å a closed loop is inherently unstable with respect to relaxation into an open loop configuration. For small loop sizes (∼7 Å) we observed this actually happening on the MD timescale.

The fact that a closed vacancy loop of sub-critical size (diameter less than ∼17.7 Å) transforms into an open vacancy loop, and then into a spherical void, was confirmed by finite-temperature MD simulations. Simulations show that a sub-critical closed vacancy loop begins to open-up on MD ∼ 1 ns timescales for temperatures around $T = 500$ K. Such a transformation also occurs at lower temperatures, but on the timescale several orders of magnitude longer.

The conversion of an open vacancy loop into a spherical void occurs *via* the diffusion of single vacancies across the

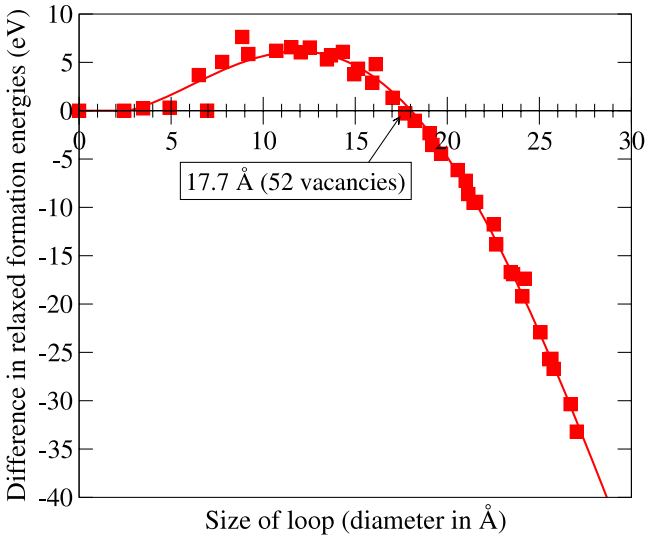

Figure 2. Difference between formation energies of closed and open $\frac{1}{2}\langle 111\rangle$ vacancy loops in Fe as a function of diameter (D–D potential).

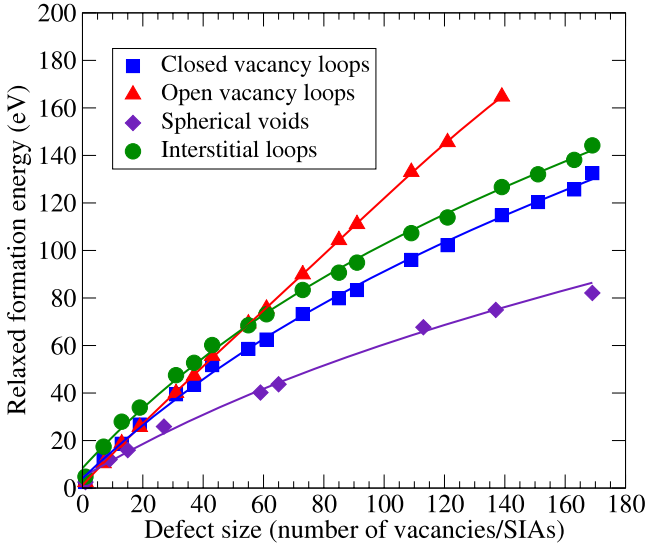

Figure 3. Variation in formation energy, as predicted by the Mendelev potential, of spherical voids and various $\frac{1}{2}\langle 111\rangle$ loop defects in Fe as a function of defect size.

internal surfaces of the open loop (a process actually observed in simulations), a general result that is expected to hold for lower temperatures albeit for longer simulation times. Hence on the timescales associated with real experiments (typically seconds or longer), sub-critical closed loops would readily transform into open loops and then into voids, even at low temperatures and certainly at room temperature.

On the other hand, the closed vacancy loops of super-critical size (diameter greater than ∼17.7 Å) can also eventually transform into voids, but the mechanism of transformation is now entirely different. By investigating the behaviour of closed super-critical size loops at temperatures greater than 1000 K we discovered that these loops shrink *via* the evaporation of individual vacancies. These free vacancies are then left to diffuse in the material and then to perhaps coalesce, forming stable voids, which then grow further by the agglomeration of vacancies. Once the loop has shrunken into the sub-critical size region it would quickly transform into a void and may then grow by sucking-in any surrounding vacancy–cluster debris that may have originally evaporated from it. It seems unlikely that super-critical loops can transform directly into spherical voids, even at high temperatures, because the transformation pathway is not straightforward. At elevated temperatures the evaporation of vacancies would occur readily and would most likely be favoured over and above more complex processes.

There is a question as to whether the effect described above is an artefact of the particular interatomic potential used. Recently, Björkas and Nordland [26] simulated recoil collision cascades in Fe using the D–D and Mendelev potentials and found that the Frenkel pair production was roughly the same under both, even though they are derived from different fitting parameters. This suggests that the Mendelev potential would produce a similar set of curves as those found for the D–D potential. We have tested this by repeating the same molecular relaxations on $\frac{1}{2}\langle 111\rangle$ defects (as well as spherical voids) using the potential of Mendelev *et al* [23]. The results are shown in figure 3. The pattern is essentially the same as that seen in results from the D–D potential, although the sub-critical region for collapsed vacancy loops is now smaller, with the intersection of the collapsed and open vacancy loops curves happening at around 30 vacancies (∼13.4 Å diameter). The main reason for this appears to be the extended range of the Mendelev potential (5.3 Å versus 4.1 Å), which causes the opposing surfaces of an open loop or planar voids to 'see' each other. This increases the relative energies of open loops when compared to their equivalent collapsed loops, leading to an earlier onset of cross-over.

What is the origin of the fundamental difference between the energies of voids, closed and open vacancy loops? The formation energy of a void containing N vacancies to a very good approximation equals its internal surface energy

$$E_{\text{void}} = 4\pi \left(\frac{3N\Omega_0}{4\pi}\right)^{2/3} \overline{W}, \tag{2}$$

where $\overline{W}$ is the average (over the low-energy orientations of surface facets) surface energy, which according to calculations [27] is of the order of 1.7 J m^{-2}, and $\Omega_0 = a^3/2 = 11.82$ Å^3 is the formation volume of a vacancy in iron, where $a = 2.87$ Å is the lattice constant. For example, the formation energy of a 102-vacancy void estimated using equation (2) is 58.1 eV, whereas the value found in simulations equals 60.9 eV using the D–D potential. Similarly, the formation energy of an open $\frac{1}{2}\langle 111\rangle$ loop is given by the sum of energies of the two free surfaces

$$E_{\text{open}} = 2\frac{a^2}{\sqrt{3}} N W_{111} + E_{\text{perimeter}}, \tag{3}$$

where $a^2/\sqrt{3}$ is the surface area corresponding to a single vacancy, and $W_{111} = 2$ J m^{-2} is the surface energy for the

(111) surface termination [27]. Estimates show that the first term in equation (3) gives the formation energy $E_{\text{open}} = 123.5$ eV for a $N = 104$ vacancy loop compared with 132.9 eV found in the D–D potential simulations. The second term in (3) describing the contribution to the formation energy from the perimeter of the loop is relatively small, and in the case of a $\frac{1}{2}\langle 111\rangle$ loop the energy per unit length of the perimeter of the loop is of the order of 0.126 eV Å^{-1}.

The formation energy of a closed dislocation loop is given by the sum of the energy stored in the elastic field loop and the core energy of the dislocation forming the perimeter of the loop [28]. Calculations based on the *anisotropic* elasticity approximation (which must be used for iron since the material is strongly elastically anisotropic even at low temperatures) give an approximate expression for the formation energy [29]

$$E_{\text{closed}} = 2\pi R^* \left[\frac{K\mathbf{b}^2}{4\pi} \ln\left(\frac{4R^*}{e\delta}\right) + F_\delta + F_c \right], \qquad (4)$$

where for the case of a $\frac{1}{2}\langle 111\rangle$ loop $K\mathbf{b}^2/4\pi \approx 0.39$ eV Å^{-1}, $F_\delta \approx 0.35$ eV Å^{-1} is the zero-temperature core-traction energy, $F_c \approx 0.47$ eV Å^{-1} is the zero-temperature anharmonic core energy, and R^* is the radius of the loop. δ is the characteristic cut-off radius for the dislocation core, which was estimated in [29] to be 0.4 nm. For a 104-vacancy loop equation (4) gives the formation energy $E_{\text{closed}} = 111.7$ eV compared with the value of 110 eV found in simulations (D–D potential). Since the diameter of a loop is proportional to the square root of the number of vacancies N, in the mesoscopic limit $E_{\text{closed}} \sim \sqrt{N}\ln N$, whereas $E_{\text{open}} \sim N$, and hence for relatively small N the formation energy of an open loop is lower than the formation energy of a closed loop. The cross-over point between the energies of closed and open vacancy loops predicted by formulae (3) and (4) is near $N = 50$, in good agreement with atomistic simulations.

We repeated the analysis of formation energies for the $\langle 001\rangle$ loops. We only considered the D–D potential for Fe, since the comparison discussed previously indicated that the Mendelev potential produces very similar results. Results are summarized in figure 4, where data for spherical voids are included for comparison. As in the $\frac{1}{2}\langle 111\rangle$ loop case, the energies of the $\langle 001\rangle$ vacancy loops are significantly higher than those of similarly sized spherical voids. The cross-over point between the energies of the open and closed loops is now significantly higher than for the $\frac{1}{2}\langle 111\rangle$ case. For loops containing fewer than about 150 vacancies (approximately 28 Å in diameter) the open loop configuration is more stable than the closed one.

Again, the formation energy of an open $\langle 100\rangle$ loop is the sum of energies of the two free surfaces

$$E_{\text{open}} = 2\frac{a^2}{2} N W_{100} + E_{\text{perimeter}}, \qquad (5)$$

where $a^2/2$ is the surface area corresponding to a single vacancy, and $W_{100} = 1.8$ J m^{-2} is the surface energy for the (100) surface termination [27]. The first term in equation (5) gives $E_{\text{open}} = 89.8$ eV for a $N = 97$ vacancy loop compared with 102.7 eV found in simulations. This shows that in the case of a $\langle 001\rangle$ vacancy loop the contribution of the perimeter term is larger than in the $\frac{1}{2}\langle 111\rangle$ open vacancy loop case, and the energy per unit perimeter length is in this case 0.184 eV/Å.

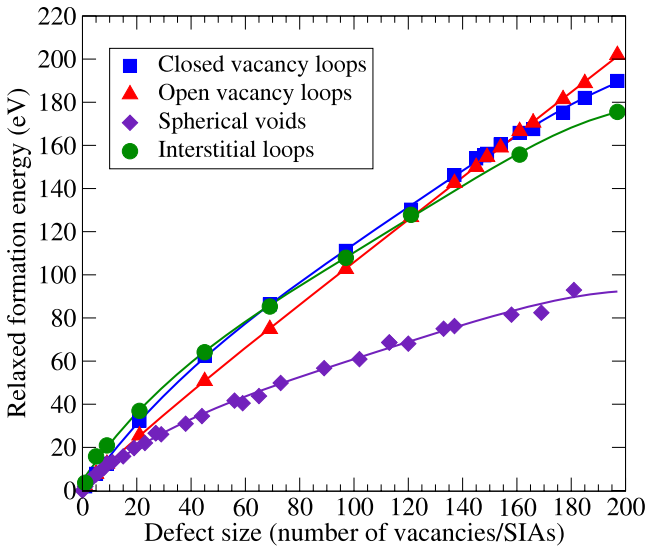

Figure 4. Variation in formation energy of $\langle 001\rangle$ mesoscopic vacancy and interstitial dislocation loops, and spherical voids in Fe plotted as a function of the number of individual defects forming the loop or a void (D–D potential).

The formation energy of a closed dislocation loop is given by equation (4), where $\mathbf{b} = (0, 0, a)$ and the anisotropic elasticity factors are [29] $K\mathbf{b}^2/4\pi \approx 0.465$ eV Å^{-1}, $F_\delta \approx 0.39$ eV Å^{-1}, and $F_c \approx 0.5$ eV Å^{-1}, and R^* is the effective radius of the loop. By substituting these values into equation (4) for a 97-vacancy loop we find the *elastic* formation energy of the loop $E_{\text{closed}} = 114$ eV compared with 111.1 eV found in atomistic simulations.

The reason for this difference in the critical size between $\frac{1}{2}\langle 111\rangle$ and $\langle 001\rangle$ closed vacancy loops can, in part, be understood through a direct comparison between the two different orientations. The graph shown in figure 5 compares the two sets of vacancy loop energies. For small defect sizes the $\langle 001\rangle$ closed loops are slightly more stable than their $\frac{1}{2}\langle 111\rangle$ equivalents. However, the difference between the two curves does not become significant until the defect size approaches 150 vacancies (30 Å diameter for $\frac{1}{2}\langle 111\rangle$, and 28 Å diameter for $\langle 001\rangle$ loops), and so this alone does not explain the large difference in the critical size. What figure 5 does indicate is that the formation energies of open loops for the two different orientations diverge significantly at fairly modest defect sizes. Density functional calculations [30] and MD simulations performed using the magnetic potential [27] have demonstrated that the (100) surface energy is significantly lower than the energy of the (111) surface. This trend is reproduced in the present simulations, where surface energies give the leading contribution to the energy of open loops. This fact is responsible for the significantly lower energy of the $\langle 001\rangle$ open loops, which in turn is the factor determining the greater cross-over size for the $\langle 001\rangle$ open/closed loop structures.

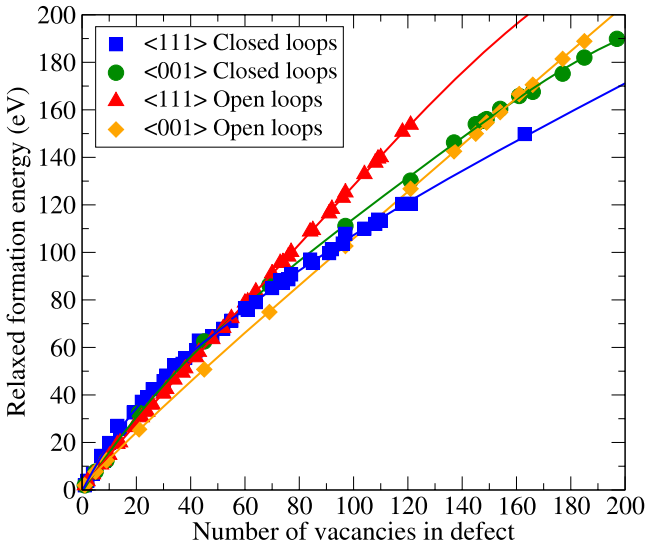

Figure 5. Comparison of energies of formation for mesoscopic vacancy loops with different Burgers vectors in iron, as predicted by the D–D magnetic potential for Fe.

In recent MD simulations of cascades in iron Calder and Bacon [31] observed the formation of rectangular ⟨001⟩ closed vacancy loops. This suggests that rectangular ⟨001⟩ clusters of vacancies are more energetically favourable than those with a more circular structure, which we have been discussing up to this point. To investigate whether this is indeed the case we have performed a series of MS relaxations using the D–D Fe potential on selected rectangular closed vacancy loops with varying size and shape for both $\frac{1}{2}\langle 111\rangle$ and ⟨001⟩ Burgers-vector orientations. Figure 6(a) displays the results for $\frac{1}{2}\langle 111\rangle$ loops. For comparison, the circular loop results of figure 1 are also shown. For the rectangular vacancy defects, the label indicates the dimensions of the loop. The first dimension is the length of the defect in the $[1\bar{1}0]$ direction in multiples of $a/\sqrt{2}$, which is the distance between the $(1\bar{1}0)$ planes in the $([1\bar{1}0], [11\bar{2}], [111])$ coordinate system. The second dimension is the length in the $[11\bar{2}]$ direction, this time in multiples of $a/\sqrt{6}$, for the same reason. From figure 6(a) it can be seen that rectangular $\frac{1}{2}\langle 111\rangle$ loops are generally higher in energy than circular closed loops of equivalent size.

If we now inspect figure 6(b), which shows the results for the ⟨001⟩ rectangular loops, an entirely different picture emerges. In this case the rectangular loop dimensions are the lengths in multiples of $a/2$ in the [100] and [010] directions, respectively. The rectangular ⟨001⟩ loops are mostly of lower energy than their circular counterparts. This suggests that they should become viable (i.e. stable compared to open loops) at a lower defect size than circular loops, and so our simulations show that rectangular ⟨001⟩ vacancy loops should form in preference to circular ones. There is also evidence to suggest that the energies of rectangular and circular ⟨001⟩ loops diverge with increasing size, with rectangular loops becoming even more energetically favourable. This agrees with experimental observations showing that the large ⟨001⟩ edge dislocation loops (either vacancy or interstitial) formed under irradiation are rectilinear in shape. For example, Masters [32], and

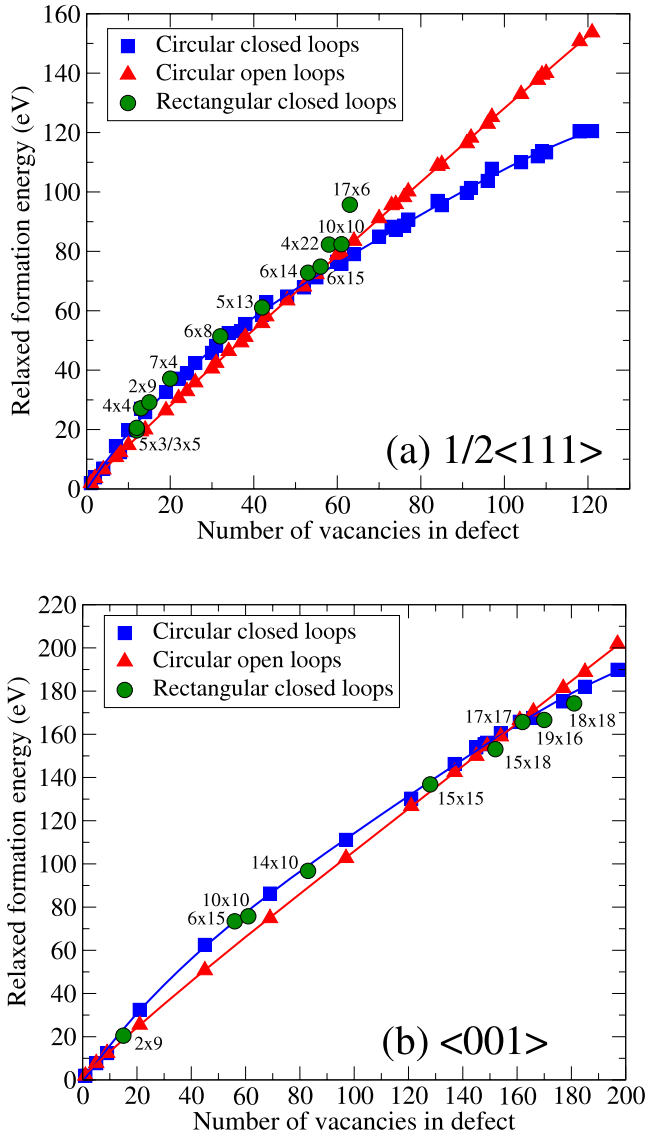

Figure 6. Comparison of formation energies of (a) $\frac{1}{2}\langle 111\rangle$ and (b) ⟨001⟩ vacancy loops of different shape in Fe (D–D potential).

Little and Eyre [33, 34] both observed the formation of large, rectangular interstitial-type dislocation loops in irradiated Fe with sides parallel to ⟨100⟩ directions and pure edge in character.

2.2. *Vacancy defects: BCC tungsten*

The formation energy analysis performed for defect clusters in Fe has been extended to defects with $(a/2)\langle 111\rangle$ Burgers vectors in tungsten. Spherical voids have also been considered. Experimental observations, see Häussermann [9], or Jäger and Wilkens [10], showed that loops of this type occur exclusively during irradiation, giving no evidence for loops with other Burgers vectors being formed. Therefore, we omitted the ⟨001⟩ loops from the tungsten study. Figure 7 summarizes the key results. Figure 7(a) shows the variation in the energy of closed vacancy–loops, interstitial loops, open vacancy loops, and spherical voids plotted as a function of defect size given

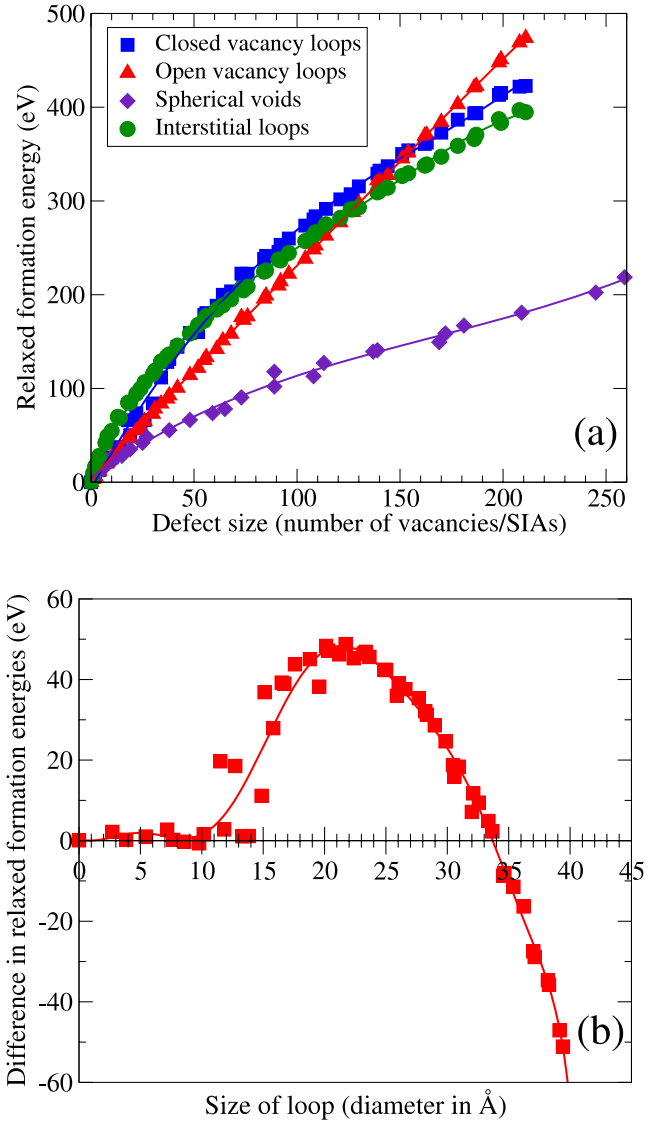

Figure 7. (a) $\frac{1}{2}\langle 111\rangle$ defect energies in W as a function of size; (b) variation of difference between closed and open $\frac{1}{2}\langle 111\rangle$ vacancy loop energies in W as a function of diameter (closed minus open).

by the number of vacancies or self-interstitials. As was the case with Fe, the open loops are more energetically favourable than their closed vacancy–loop equivalents for small defects. There is a critical size above which the reverse becomes true.

Figure 7(b) shows how the difference in the formation energy of closed and open $\frac{1}{2}\langle 111\rangle$ vacancy loops varies as a function of the diameter of a loop. The critical size, above which the closed loops are energetically more stable than the open ones, is about 34 Å, corresponding approximately to a 157-vacancy defect. This is considerably larger than in Fe (18 Å, ∼50 vacancies). Similarly to the case of Fe, the spherical voids are the most stable configuration for a vacancy cluster of any size (see figure 7(a)), but the large difference between the energy of this structure and the equivalently sized (in terms of the number of vacancies) planar defects means that the vacancy loops *of any kind* in tungsten are highly unstable and readily transform into spherical voids through surface vacancy diffusion and/or vacancy evaporation.

2.3. Self-interstitial defects

Figure 1 shows that except at very small defect sizes (less than 10 vacancies/interstitials), under the D–D potential in Fe $\frac{1}{2}\langle 111\rangle$ interstitial loops are of lower energy than equivalently sized closed vacancy loops. This is repeated for $\langle 001\rangle$ loops in Fe (figure 4) and in W (figure 7(a)). Since the difference between energies of closed vacancy loops and interstitial loops is related to the length of the perimeters of the loops, these observations suggest that in the limit of large defect size the core energy of the curved dislocation forming the perimeter of a vacancy loop is greater than that of an interstitial loop of the same size. The difference between the interstitial and closed vacancy loop curves in all the graphs of figures 1, 4, and 7 increases slightly with defect size. This is consistent with the concept of the energy per unit perimeter length being greater for vacancy loops. Puigvi *et al* [19] observed this divergence in atomic simulations of defects in Fe, and found that the relative energies of interstitial and vacancy loops are sensitive to the choice of interatomic potential. Using the long-range pair potential of Osetsky *et al* [35] they found the same relationship for $\frac{1}{2}\langle 111\rangle$ loops in Fe as presented here, but with the Ackland *et al* [36] many-body potential the reverse situation was observed, namely that vacancy loops were of lower energy than their interstitial counterparts. We observe a similar phenomenon in our simulations. Under the Mendelev potential for Fe, we see that the $\frac{1}{2}\langle 111\rangle$ interstitial loops are higher in energy than equivalent collapsed vacancy loops (see figure 3), which is opposite to the results under D–D.

Both interstitial and closed vacancy loops are related to an edge dislocation; one with the extra half-plane inside the loop (interstitial), and one with it on the outside (*closed* vacancy loop). This results in the relaxed configurations of equivalently sized interstitial and vacancy loops being difficult to distinguish from one another.

Clearly, it is not possible to observe the asymmetry between the two structures, which exists, by direct viewing of their constituent atoms. However, by analysing the strains in directions parallel to the burgers vector of a loop we can gain some insight. In the $([1\bar{1}0], [11\bar{2}], [111])$ coordinate system the atoms can be grouped according to which [111] atomic string they belong to. For $\frac{1}{2}\langle 111\rangle$ loops we can then calculate the strain in the [111] direction between each pair of adjacent atoms of a particular string, using the equation:

$$\varepsilon_n^{[111]} = \frac{\delta\ell}{\ell_0} = \frac{\left(x_n^{[111]} - x_{n-1}^{[111]} - \frac{\sqrt{3}}{2}a\right)}{\frac{\sqrt{3}}{2}a}, \qquad (6)$$

where $\varepsilon_n^{[111]}$ is the strain associated with atom n in the [111] direction relative to the $n-1$ atom neighbouring it. $\delta\ell$ is the extension, which in this case is the difference between the current separation of the atoms in [111] $(x_n - x_{n-1})$ and their original separation in a perfect lattice ℓ_0. For the [111] direction this is $\sqrt{3}/2$ times the lattice parameter a. In a perfect lattice these strains are all close to zero, but if the string passes

through a defect then we can expect some of the strain values to be either negative (compression) or positive (tension).

In figure 8 the 'maximum strain magnitudes' for each string have been calculated for equivalent 199 interstitial and super-critical vacancy $\frac{1}{2}\langle 111\rangle$ loops in W. In the graph the maximum strains are plotted as a function of the corresponding string's radial distance from the centre of the loop. To aid visualization we have plotted the strings lying in the positive $(1\bar{1}0)$ half-plane, relative to the loop centre, on the right of the graph, and those in the negative half-plane to the left. At both ends of the graph the strains are essentially zero, and these correspond to strings on the outside of the loops that are so far from the defects that they experience little or no distortion. As the strings get closer to the edges of the loops the strains they experience become greater, reaching a maximum (either positive or negative) at the approximate position of the edges at around ±19 Å in these 38 Å diameter loops. As we move through the interior of the loops the strains fall away from their maximums at the edges and are near zero again at the centres, before increasing again towards the other edge.

We note that the strains in the defect centres are not as close to zero as those on the outside, far from the loop. This is due to the combined perimeter effect from all directions (as opposed to just one direction for strings exterior to the defect) which leads to some strain (less than 5%), even at the centre of the loop. Only in very large loops the edges of the loops are far away from each other to experience nearly no strain, however this condition is not reached even in a 463-vacancy closed $\frac{1}{2}\langle 111\rangle$ loop in Fe (5.3 nm diameter). We note that the magnitudes of the tensions are roughly 10% greater than the maximum compressive strains. For the closed vacancy loop (blue diamonds) the strains become rapidly more negative (compressive) as the strings get closer to the loop edge from the outside. The strains reach a maximum compression of almost 15% before switching to tensions (positive strains) of the order of 25% at the loop edge, which are associated with the absence of atoms. The tensions fall to nearly zero within 2 Å of the edge.

In the case of the interstitial loop (red triangles) there are extra atoms inside the loop, which causes the mirror image of the strain patterns seen for the vacancy loop. This time the compressions increase to 15% from inside the loop (which again persist at a less than 5% level to the centre of the loop), which then switches to the 25% tension on the outside of the loop, which drops to less than 3% within about 2 Å. We see that there is clear asymmetry in the structure of interstitial and vacancy dislocation loops.

The structural similarity between interstitial and vacancy loops, as illustrated by the graph in figure 8, suggests that the thermal migration of equivalently sized stable interstitial and vacancy loops might be expected to be quite similar. We have investigated this issue by measuring the respective diffusion coefficients using long-time finite-temperature MD simulations. As reported previously by Osetsky *et al* [37, 38], we find that vacancy loops do migrate on similar timescales as interstitial loops, though at a systematically lower rate.

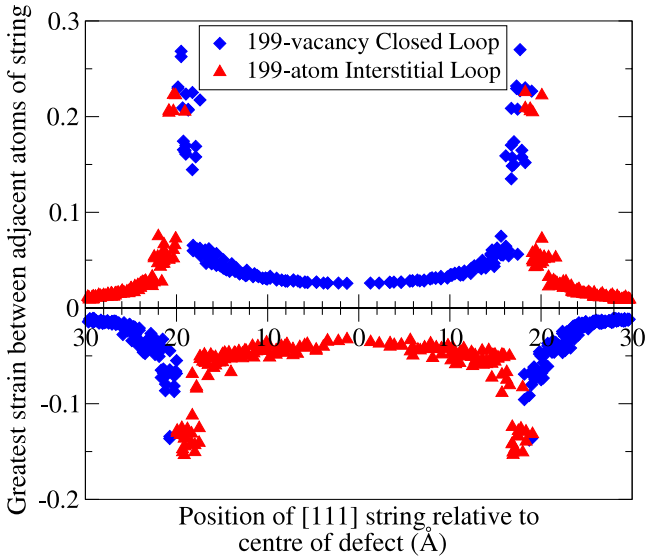

Figure 8. Variation of maximum strain through $\frac{1}{2}\langle 111\rangle$ closed vacancy and interstitial loops in W.

3. Comparison with experiment

It is important to appreciate the difference between the length-scales of our simulations and experimental observations. Whilst a mesoscopic loop might be considered as small in experiments, such a defect contains several hundred vacancies or self-interstitial atoms and is in effect very large in the context of an MD/MS simulation.

When comparing the results of the simulations performed to what has been seen in transmission electron investigations of irradiated samples, one must keep in mind that in the few nm defect size range, only the long-range strain fields associated with prismatic dislocation loops (i.e. closed vacancy loops) can be resolved [3, 9]. Spherical voids do not carry a large strain field, and thus with the exception of very large cavities containing several hundred vacancies, such voids, if present at equilibrium, would be fairly difficult to see in transmission electron microscope (TEM) images. Thus the prediction that at loop diameters less than a critical value it is the open loops, transforming into spherical voids, that are the most energetically favourable configurations may be relatively difficult to verify by means of electron microscope observations. Recently, Yao *et al* [3] improved the technique for imaging small voids and confirmed the presence of numerous small voids in iron foils irradiated with energetic ions.

There is also the issue of to what regions of a material our simulations correspond. As discussed in section 2.1, validation simulations indicate that our results are most appropriate to defects in the bulk of irradiated materials. In particular, they are not directly applicable to the region close to the surface of thin foils (typically ∼10 nm thick [3]), where in-plane dislocation loops are strongly attracted to the surface leading to a so-called *depleted zone*. However they can be compared to the deeper damage regions of some experiments, where surface effects are not significant. Also, if a dislocation loop

(spherical and planar voids have no elastic fields and so are unaffected by surfaces in general) lies perpendicular to the surface its elastic field would not interact with the surface and in these circumstances our simulations would apply to the loop regardless of its distance to a boundary.

Our results offer a likely explanation for the low closed vacancy loop yield observed using electron microscopy in irradiation-induced cascade experiments, which is typically of the order of 1% or lower in self-ion irradiation experiments, and certainly much lower than in similar experiments on fcc metals [7]. In order to produce a long-lived closed vacancy loop, the number of vacancies in a cascade must be sufficiently high-enough so that upon collapse a super-critical (more than around 30–50 vacancies in size) loop is formed. In most cascades the total number of vacancies is too low to produce a stable loop, since any closed loop forming in the sub-critical size region will be unstable and will transform rapidly to an open loop structure and finally to a small spherical cavity.

Positron annihilation lifetime spectroscopy experiments on neutron irradiated copper and iron [39, 40], have detected the production of small (typically less than 1 nm in diameter in the case of a spherical cavity) void defects. In Fe, these voids are produced in large numbers (on the order of 10^{24} defects per square metre [40]) at relatively low irradiation doses, which illustrates their preferential formation compared to vacancy dislocation loops, in agreement with our simulations. Thus, in the majority of irradiation conditions, and certainly in neutron irradiation, most of the vacancy defects produced in cascade collapse events in Fe are voids, with an occasional super-critical vacancy loop. Only under heavy-ion irradiation, where the cascades are smaller but have a higher vacancy density, does the yield of vacancy dislocation loops becomes more significant [3].

For the case of tungsten, the situation is different. In experiments of Häussermann [9], where W (and Mo) was irradiated using energetic gold ions, the $\frac{1}{2}\langle 111\rangle$ vacancy loops were found to have an average diameter of between 27 and 46 Å, depending on the sample used in experiments. Thus vacancy loops with diameters less than the critical size of 34 Å were observed, in contradiction with our simulation results.

A likely reason for the discrepancy is the strongly non-equilibrium nature of the defects generated by irradiation in tungsten. The time taken for a particular cascade event to reach equilibrium can be estimated by considering the timescale of migration of the vacancies produced during the cascade expansion phase. During collapse, which leads to the formation of voids and other defects, these vacancies migrate across the volume of the cascade, and therefore their motion is the rate determining factor for reaching equilibrium. We can estimate the characteristic equilibration time τ as:

$$\tau \approx \frac{L_{\text{cascade}}^2}{D_{\text{v}}}, \tag{7}$$

where L_{cascade} is the size of a cascade, typically of the order of 0.5×10^2 Å, and D_{v} is the diffusion coefficient for a single vacancy at temperature T, given by the Arrhenius equation:

$$D \approx d^2 \nu_0 \exp\left[-\frac{E_{\text{a}}}{k_{\text{B}}T}\right]. \tag{8}$$

Here the attempt frequency ν_0 can be approximated as the Debye frequency ω_{D} divided by 2π. ω_{D} is calculated from the Debye temperature T_{D} via

$$\omega_{\text{D}} = \frac{k_{\text{B}}T_{\text{D}}}{\hbar}. \tag{9}$$

For Fe $T_{\text{D}} = 420$ K and for W it is 310 K [41], giving the Debye frequencies of 8.75×10^{12} and 6.46×10^{12} s^{-1}, respectively. d is the jump distance, which for a bcc lattice is $\frac{\sqrt{3}}{2}a$. The activation energy E_{a} for vacancy migration used in these calculations was 0.67 eV for Fe [42] and 1.78 eV for W [43]. Assuming that $T = 300$ K (room temperature) we find that for Fe this leads to the characteristic time of around 8 s whereas for W the result is the order of 4×10^{20} s, which is equivalent to more than 10^{13} years!

The above estimate explains why in irradiation experiments of tungsten the size range of the observed vacancy loops includes diameters below the critical size predicted by our simulations. Whereas in Fe it is realistic to expect the experimental observations to be of equilibrium configurations, it is virtually impossible for this to be the case in experiments on tungsten because the system is not able to reach equilibrium over normal timescales at room temperature. Thus the configurations observed in experiments on tungsten at room temperature do not represent the minimum energy configuration required for direct comparison with the simulation results presented here.

The characteristic time for Fe obtained from our estimate above is a little longer than the timescale for the formation and evolution of vacancy dislocation loops observed in the recent irradiation experiments by Yao *et al* [3], which was of the order of 0.1 s. Kinetic Monte Carlo (kMC) simulations of cascade evolution in Fe by Hudson *et al* [44] have also indicated that the single vacancy concentration falls to zero on this 0.1 s timescale at $T = 500$ K as a result of diffusion followed by clustering or recombination with self-interstitial atoms.

4. Concluding remarks

In conclusion, in the present work we have investigated both the 0 K stability of vacancy and interstitial defects structures and the thermal migration properties of vacancy and interstitial prismatic loops. Analysis of the formation energy of vacancy clusters has confirmed that spherical voids are the most energetically favourable configuration for a cluster of any given number of vacancies. Hence the vacancy loop structures seen experimentally represent metastable configurations, which, given enough time and sufficient thermal activation, should evolve into the void structure. Additionally, the stability investigation also suggests that there is a critical size below which these vacancy loops become even more energetically unfavourable. In this region the open loop structure is more stable, although it has a tendency to transform into a spherical void at modest temperatures via the diffusion of single vacancies across its surface. For Fe, this is in good agreement with recent experimental observations by Yao *et al* [3], where the smallest loops observed in iron were no smaller than around 2 nm or 20 Å in diameter. For the case of W, experiments [9] indicate the presence of vacancy loops

below the stability threshold found in the simulations. This observation can be rationalized by realizing that in W, due to its extremely low vacancy diffusion coefficient, the cascade evolution cannot proceed to equilibrium conditions on the typical experimental timescale.

Acknowledgments

We gratefully acknowledge stimulating discussions with Dr Z Yao, Dr M L Jenkins, and Dr M A Kirk. This work was supported by the UK Engineering and Physical Sciences Research Council, by EURATOM, and by EXTREMAT integrated project under contract number NMP3-CT-2004-500253.

References

[1] Arakawa K, Hatanaka M, Kuramoto E, Ono K and Mori H 2006 *Phys. Rev. Lett.* **96** 125506
[2] Arakawa K, Ono K, Isshiki M, Mimura K, Uchikoshi M and Mori H 2007 *Science* **318** 956–9
[3] Yao Z, Hernandez-Mayoral M, Jenkins M L and Kirk M A 2008 *Phil. Mag.* at press
[4] Woo C H, Semenov A A and Singh B N 1993 *J. Nucl. Mater.* **206** 170–99
[5] Woo C H 1999 *J. Comput.-Aided Mater. Des.* **6** 247–75
[6] English C A and Jenkins M L 1987 *Mater. Sci. Forum* **15–18** 1003–22
[7] Jenkins M L, Kirk M A and Phythian W J 1993 *J. Nucl. Mater.* **205** 16–30
[8] Jenkins M L and Kirk M A 2001 *Characterization of Radiation Damage by Transmission Electron Microscopy* (Bristol: Institute of Physics Publishing)
[9] Von Häussermann F 1972 *Phil. Mag.* **25** 583–98
[10] Jäger W and Wilkens M 1975 *Phys. Status Solidi* a **32** 89–100
[11] Jenkins M L, Nicol A C and Kirk M A 2001 *Mater. Res. Soc. Symp. Proc.* **650** R1.3
[12] Horiki M, Yoshiie T, Iseki M and Kiritani M 1999 *J. Nucl. Mater.* **271/272** 256–60
[13] Horiki M, Yoshiie T, Xu Q, Iseki M and Kiritani M 2000 *J. Nucl. Mater.* **283–287** 282–5
[14] Matthai C C and Bacon D J 1985 *J. Nucl. Mater.* **135** 173–80
[15] Soneda N and Diaz de la Rubia T 1998 *Phil. Mag.* A **78** 995–1019
[16] Beeler J R 1983 *Radiation Effects Computer Experiments* (Amsterdam: North-Holland)
[17] Soneda N, Ishino S and Diaz de la Rubia T 2001 *Phil. Mag. Lett.* **81** 649–59
[18] Calder A F, Bacon D J, Barashev A V and Osetsky Yu N 2008 *Phil. Mag. Lett.* **88** 43–53
[19] Puigvi M A, Osetsky Yu N and Serra A 2003 *Phil. Mag.* **83** 857–71
[20] Osetsky Yu N, Bacon D J, Serra A, Singh B N and Golubov S I 2000 *J. Nucl. Mater.* **276** 65–77
[21] Dudarev S L and Derlet P M 2005 *J. Phys.: Condens. Matter* **17** 7097–118
[22] Derlet P M and Dudarev S L 2007 *Prog. Mater. Sci.* **52** 299–318
[23] Mendelev M I, Han S, Srolovitz D J, Ackland G J, Sun D Y and Asta M 2003 *Phil. Mag.* **83** 3977–94
[24] Derlet P M, Nguyen-Manh D and Dudarev S L 2007 *Phys. Rev.* B **76** 054107
[25] Johnson R A 1967 *Phil. Mag.* **16** 553–64
[26] Björkas C and Nordland K 2007 *Nucl. Instrum. Methods* B **259** 853–60
[27] Van Zwol P, Derlet P M, Van Swygenhoven H and Dudarev S L 2007 *Surf. Sci.* **601** 3512–20
[28] Bacon D J, Bullough R and Willis J R 1970 *Phil. Mag.* **22** 31–45
[29] Dudarev S L, Bullough R and Derlet P M 2008 *Phys. Rev. Lett.* **100** 135503
[30] Spencer M J S, Hung A, Snook I and Yarovsky I 2002 *Surf. Sci.* **513** 389–98
[31] Calder A F and Bacon D J 2006 private communication from D Bacon
[32] Masters B C 1965 *Phil. Mag.* **11** 881–93
[33] Little E A and Eyre B L 1973 *Met. Sci.* **7** 100–2
[34] Little E A and Eyre B L 1973 *J. Microsc.* **97** 107–11
[35] Osetsky Yu N, Mikhin A G and Serra A 1995 *Phil. Mag.* A **72** 361–81
[36] Ackland G J, Bacon D J, Calder A F and Harry T 1997 *Phil. Mag.* A **75** 713–32
[37] Osetsky Yu N, Bacon D J and Serra A 1999 *Phil. Mag. Lett.* **79** 273–82
[38] Osetsky Yu N, Bacon D J, Serra A, Singh B N and Golubov S I 2003 *Phil. Mag.* **83** 61–91
[39] Eldrup M, Singh B N, Zinkle S J, Byun T S and Farrell K 2002 *J. Nucl. Mater.* **307–311** 912–7
[40] Eldrup M and Singh B N 2003 *J. Nucl. Mater.* **323** 346–53
[41] Ashcroft N W and Mermin N D 1976 *Solid State Physics* (London: Thomas Learning)
[42] Fu C-C, Williame F and Ordejón P 2004 *Phys. Rev. Lett.* **92** 175503
[43] Nguyen-Manh D, Horsfield A P and Dudarev S L 2006 *Phys. Rev.* B **73** 020101
[44] Hudson T S, Dudarev S L, Caturla M-J and Sutton A P 2005 *Phil. Mag.* **85** 661–75